

## Insights into the origins, molecular characteristics and distribution of iron-binding ligands in the Arctic Ocean

Tatiana Williford<sup>1\*</sup>, Rainer M.W. Amon<sup>1,2\*</sup>, Ronald Benner<sup>3</sup>, Karl Kaiser<sup>2</sup>, Dorothea Bauch<sup>4,5</sup>, Colin Stedmon<sup>6</sup>, Ge Yan<sup>2#</sup>, Sally A. Walker<sup>1†</sup>, Michiel Rutgers van der Loeff<sup>7</sup>, Maarten B. Klunder<sup>8‡</sup>

<sup>1</sup>Texas A&M University, USA, <sup>2</sup>Texas A&M University Galveston Campus, USA, <sup>3</sup>University of South Carolina, USA, <sup>4</sup>Leibniz-Laboratory, University of Kiel CAU, Germany, <sup>5</sup>GEOMAR Helmholtz Centre for Ocean Research, Germany, <sup>6</sup>Technical University of Denmark, Denmark, <sup>7</sup>Alfred-Wegener Institute for Polar- und Marine Research, Germany, <sup>8</sup>Royal Netherlands Institute for Sea Research, Netherlands

\*corresponding authors (tatiana.williford@gmail.com; amonr@tamu.edu)

#currently at: Institute of Deep-Sea Science and Engineering, Chinese Academy of Sciences, Sanya, China; †currently at: Applied Research Laboratories, University of Texas at Austin, USA;

‡currently at: Department of Environmental Fate, CTGB, Ede, The Netherlands

### Abstract

Dissolved lignin phenols, chromophoric dissolved organic matter (DOM), and in situ fluorescence were determined in waters of the Laptev Sea and major Arctic basins, and they were compared with dissolved iron (dFe) distributions to elucidate the sources, molecular characteristics and distributions of iron-binding ligands in the Arctic Ocean. In the Transpolar Drift region (TPD), concentrations of dFe were positively correlated with concentrations of lignin phenols and multiple optical proxies of DOM composition and source. Strong relationships between dFe and visible and ultraviolet wavelength fluorescent DOM indicated that vascular plant and algal-derived DOM contributed to the dFe-ligand pool. These observations are consistent with previous studies suggesting the association of dFe with humic terrigenous and marine organic ligands. The primary sources of iron-binding ligands appear to be the riverine discharge of terrigenous DOM, marine organic matter produced on the shelves, and degradation products of plankton-derived organic matter in the shelf sediments. A stronger relationship between dFe and visible wavelength CDOM fluorescence than with lignin phenols suggested the presence of multiple terrigenous ligands, such as aromatic tannins. The aromatic nature of these

terrigenous ligands was indicated by a strong relationship between dFe and the absorption coefficient at 254 nm. A strong negative correlation between the p-hydroxyl to vanillyl lignin phenols ratio and dissolved iron concentrations indicated recently-discharged terrigenous DOM (tDOM) was an important source of iron-binding ligands. Given the strong relationships of marine and terrigenous DOM with dissolved iron, iron-binding functional groups appear to occur in diverse molecules of multiple sources. Examples of such iron-binding functional groups included catechols and carboxylates found in lignins and tannins of terrigenous origins and carboxyl-rich alicyclic molecules (CRAM) of terrigenous and marine origins. The observed dFe distributions in the Arctic Ocean could not be explained by the presence of a single ligand type, but rather by a potpourri of ligand molecules of varying concentrations and binding strengths. This molecular diversity of ligands and associated binding strengths ultimately controls the distribution and transport of dFe in the Arctic Ocean and beyond.

#### Keywords

Dissolved organic matter; Iron; Organic ligands; Complexation; Biomarkers; Optical properties; CDOM; Arctic Ocean

#### 1. Introduction

As a relatively small basin (1.3% of the global ocean volume), the Arctic Ocean receives a disproportionately high fraction (10%) of global river discharge, giving dissolved organic matter (DOM) in the Arctic Ocean a strong terrigenous signal (Opsahl et al. 1999, Amon 2004, Benner et al. 2005, Anderson and Amon, 2015; Kaiser et al. 2017). Fluvial discharge is an important source of both DOM and trace metals to the Arctic Ocean (Batchelli et al. 2010; Klunder et al, 2012a; Krachler et al. 2012; Whitby et al. 2020). Recent studies demonstrate that peat-derived, lignin-containing humic substances are not only efficient in mobilizing iron from the soils due to the functional groups reacting with ferrous oxides, but they are also carriers of riverine iron to the open ocean (Krachler et al. 2012). This is consistent with elevated concentrations of iron and humic substances serving as iron-binding ligands, as recently reported for the Transpolar Drift (TPD) region (Slagter et al. 2017). A prominent role for humic substances as iron-binding ligands has also been suggested for the halocline layer in the Canada Basin, where Nakayama et al. (2011) detected elevated dissolved iron concentrations along with

the optical fingerprints of humic substances. Some Arctic shelf seas, like the Barents and the Kara Seas, were characterized by lower dissolved iron concentrations, but elevated iron concentrations were found in the Laptev Sea, particularly in bottom waters (Klunder et al. 2011).

Iron is an essential nutrient for marine organisms, but it has poor solubility in seawater, and acquiring iron in oxic waters is challenging for most marine microorganisms. The biogeochemistry of DOM and trace metals is intrinsically linked due to organic ligands that retain metals such as iron in solution, thereby facilitating transport by preventing iron scavenging and influencing iron bioavailability (Rijkenberg et al. 2018; Hassler et al. 2011; Laglera et al. 2019). Siderophores, carbohydrates, and humic substances are viewed as potential iron-binding ligands in the ocean (Benner 2011; Hassler et al. 2011; Laglera et al. 2019). Siderophores are strong ligands synthesized by marine bacteria to specifically bind iron, but they are found in very low concentrations in natural waters (Mawji et al. 2008). Other organic molecules contain functional groups similar to those found in siderophores. Examples of such functional groups are catechols and carboxylates that are present in naturally occurring biochemicals found in dissolved humic substances, and they can form iron-binding complexes of varying binding strengths and varying resistance to photodegradation (Barbeau et al. 2003). Catecholates are prone to photooxidation in the free form, but are more resistant when complexed to iron, while  $\alpha$ -hydroxy carboxylate groups are stable as the free acid, but prone to photooxidation when coordinated to iron (Barbeau et al. 2001; 2003). Carboxyl-rich alicyclic molecules (CRAM) are another naturally occurring group of molecules that are potentially important ligands in the ocean iron cycle (Hertkorn et al. 2006; Hassler et al. 2019; Whitby et al. 2020).

In this paper, we explore how a diverse group of molecules in DOM can serve as binding sites for iron complexation in different water masses of the Arctic Ocean, and how they affect dissolved iron distributions and transport. Lignin phenols are well-established biomarkers for tracing terrigenous DOM in the ocean (Opsahl and Benner, 1997; Opsahl et al 1999; Benner et al. 2005, Kaiser et al. 2017), and we use these biomarkers along with the measurements of the optical properties of DOM to investigate the relationships among potential organic ligands and dissolved iron concentrations in specific water masses. Studying the Arctic Ocean, which is heavily influenced by river discharge and shelf-basin interactions, can provide insights about the origins, binding strengths, and distributions of organic ligands from various sources.

## 2. Methods and data

### 2.1. Sampling

Samples were collected during the Ark-XXII/2 expedition on board the research ice breaker Polarstern (July-October 2007). *In situ* CDOM fluorescence, water samples, and hydrographic data (conductivity, temperature, and depth measured using two SeaBird CTDs (Schauer, 2008) were collected from several sections across the Nansen Basin, Amundsen Basin, and Makarov Basin (Fig.1). The western portion of section A (A1) starts on the Barents Sea shelf (stations 227-260) and the eastern portion (A2) starts in the St. Anna Trough (stations 261-276), both crossing the Nansen Basin. This section is dominated by the inflowing Atlantic water. Section B stretches from the Kara Sea shelf break across the Nansen Basin, the Amundsen Basin, and the Lomonosov Ridge into the Makarov Basin and the northern Canada Basin (stations 279-342). Section B provides observations of the TPD region. Section C starts on the Laptev Sea shelf and follows the Gakkel Ridge which separates the Nansen and Amundsen Basins, providing an opportunity to investigate shelf processes (stations 346-411).

### 2.2. Dissolved organic carbon and optical properties

Samples for dissolved organic carbon (DOC) analysis and optical properties were filtered through pre-combusted 0.7 mm GF/F filters (Whatman) and sealed in pre-combusted glass ampoules on board. The samples for DOC and optics were analyzed within one year of collection. For the DOC analysis, the samples were frozen at -20°C in glass ampoules until analysis at the home laboratory. DOC concentrations were determined using a modified MQ-1001 TOC Analyzer or a Shimadzu TOC-V CSH/CSN. The calibration curve was created daily using potassium hydrogen phthalate, and the accuracy was ensured by measuring deep-sea standards (Hansell, 2005). DOC concentrations were calculated using the average of five replicate sample injections, followed by a Milli-Q blank subtraction.

*In situ* CDOM fluorescence was measured with a backscatter fluorometer (excitation 350-460 nm/emission 550 nm HW 40nm; Dr. Haardt Optik Mikroelektronik). Absorbance was measured from 240 to 800 nm on a Shimadzu UV-1800 dual-beam ultraviolet-visible

spectrophotometer using a 5 cm quartz cuvette and pure water as a blank. The raw absorbance was baseline corrected by subtracting an offset- exponential fit of the absorbance spectrum over the range from 300 nm to 650 nm (Stedmon et al. 2000). The corrected absorbance ( $A_\lambda$ ) was converted to Napierian absorption coefficients ( $a_\lambda$ ) for each wavelength,  $\lambda$ , with the following formula:

$$a_\lambda = \ln(10) \frac{A_\lambda}{L}, \quad (1)$$

where  $L$  is the length of the cuvette in meters. Here we use the absorption at 254 ( $a_{254}$ ) and 350 nm as a proxy for CDOM concentration.

The spectral slope between 275 nm and 295 nm ( $S_{275-295}$ ) can be used as a tracer of the percent terrigenous dissolved organic carbon in river-influenced ocean margins (Fichot & Benner, 2012) and an indicator of photooxidation and photobleaching (Helms et al. 2008).  $S_{275-295}$  was computed using a linear fit of the log-linearized  $a_\lambda$  spectrum over the spectral range between 275 and 295 nm and are reported here with units of  $\text{nm}^{-1}$ .

Spectral organic matter fluorescence was measured with a Photon Technologies International spectrofluorometer (Quanta Master-4 SE) using a 1 cm quartz cuvette with excitation and emission slit widths of 5 nm. Excitation-emission matrix scans (EEMs) for each sample covering emission from 300 to 600 nm (2 nm increment) and excitation wavelengths ranging from 240 to 450 nm (5 nm increment). Daily pure water (Milli-Q) blanks were obtained and subtracted to remove water scattering peaks. Measured data were spectrally corrected for instrument bias and subsequently, Raman calibrated using the pure water blanks. The fluorescence was characterized using Parallel Factor (PARAFAC) analysis on normalized EEMs using the drEEM toolbox (Murphy et al. 2013) and the normalization was reversed after the model fitting so that the fluorescence intensities of each component are in Raman Units.

Four outlier samples were identified to disproportionally bias the PARAFAC modeling and therefore removed. The final Ark-XXII/2 dataset consisted of 354 EEMs and a five-component model was found optimal based on spectral loadings, residual examination, and split-half validation using a convergence criterion of  $1e^{-8}$  (Fig.2). The components were labeled based on their emission maxima: C<sub>428</sub>, C<sub>482</sub>, C<sub>408</sub>, C<sub>315</sub>, and C<sub>302</sub>.

## 2.3 Lignin phenol analysis

For lignin analysis 10–15 L seawater samples were filtered using a 0.2 mm pore size NuclePore filter cartridge, acidified to pH 2.5 using concentrated HCl (reagent grade), followed by solid-phase extraction using C18 cartridges (Varian MegaBond 10 g, 60 mL, Louchouart et al. 2000). Cartridges were stored at -20°C until extracted with 30 ml of methanol at 4 ml min<sup>-1</sup> in the lab. The extracts were preserved at -20 °C until lignin analysis in the home laboratory. Lignin phenol analysis was performed following the method of Yan and Kaiser (2018 a, b). It allows the quantification of dissolved lignin phenols in small volumes of seawater using alkaline CuSO<sub>4</sub> at 150°C at 5–100 µg of sample organic carbon content. Ultra-high performance liquid chromatography with mass spectrometry detection in dynamic Multiple Reaction Monitoring mode and isotopically-labeled surrogate standards were used for the detection and quantification of monomeric lignin phenols.

The sum of concentrations of nine lignin phenols (TDLP9) is reported in this study: p-hydroxybenzaldehyde (PAL), p-hydroxyacetophenone (PON), p-hydroxybenzoic acid (PAD), vanillin (VAL), acetovanillone (VON), vanillic acid (VAD), syringaldehyde (SAL), acetosyringone (SON), syringic acid (SAD). The ratios of syringyl (SAD, SAL, SON) to vanillyl (VAL + VAD + VON) phenols (S/V) and p-hydroxyl (PAL + PAD + PON) to vanillyl phenols (P/V), are commonly used as a source or diagenetic indicators (Amon et al. 2012). In Arctic rivers, these lignin monomer ratios exhibit spatial and seasonal variability, but in general S/V ratios are higher in the Yukon, Ob, and Kolyma (0.4–0.6), relative to the Mackenzie, Lena, and Yenisei (<0.3) (Amon et al. 2012). The ratio of P/V is also used as diagenetic indicators, as they increase with increasing DOC-age (Amon et al. 2012). In this study, we use the new method for lignin phenols analysis (Yan and Kaiser, 2018a, b). The phenols concentrations for the marine samples are comparable between the new and the old methods, although the new method results in lower acid/aldehyde ratios (Yan & Kaiser, 2018b). The limit of detection ranges from 10 to 87 femtomoles for individual lignin phenols (Yan & Kaiser, 2018b).

#### *2.4 Additional data.*

The dissolved iron (dFe) data used in this study were obtained from Klunder et al. (2012a, b; also available in Schlitzer et al., 2018), we limited it to the upper 500 meters. The samples for iron analysis were collected from the GO-FLO bottles in a class 100 clean room environment and filtered through a 0.2 mm filter cartridge (Sartrobran-300, Sartorius) under

nitrogen pressure (1.5 atm.) (Klunder et al. 2012a, b; the GEOTRACES intermediate data product 2017)

Table 1. The optical and chemical parameters reported in this study.

Parameter	Description
CDOM	<i>in situ</i> fluorescence from Dr. Haardt fluorometer. Units: volts
$a_{254}, a_{350}$	Absorption coefficients at 254 and 350 nm are commonly used proxies for CDOM abundance and origin. Units: $m^{-1}$
TDLP9	Sum concentration of 9 lignin phenols based on LC/MS. Units: nmol/L
$S_{275-295}$	Exponential spectral absorption slope. Proxies for CDOM character (origin and photooxidation). Units $nm^{-1}$
SUVA	The specific UV absorbance at 254 nm. Decadic absorption at 254 normalized to the DOC concentration. Surrogate for aromaticity Units: $m^2 g^{-1} C$
S/V	Proxy for taxonomic source: high S/V - angiosperm, low S/V – gymnosperms. No units
P/V	Increase with DOM age, increase with sun exposure, an indicator for bryophyte vegetation in peatlands, Ob river estuary, sensitive to changes in river flow. No units
dFe	Dissolved iron concentration (Klunder et al. 2012a, b). Units: nmol/L

### 3. Results

Surface water *in situ* CDOM fluorescence reflects the general horizontal circulation patterns in the Arctic Ocean (Fig.1). The Nansen Basin is influenced by AW inflow and has the lowest *in situ* fluorescence, which can be observed in sections A and B. The CDOM-enriched fluvial discharge is partially observed on the Laptev Sea shelf (section C), as the river influenced coastal waters travel towards the east, contained on the shelves by the Atlantic water boundary current. These high CDOM coastal waters are entrained into the TPD east of section C, in the East Siberian Sea or the Chukchi Sea (Alkire et al., 2019) and flow across the Central Arctic

Ocean as part of the TPD. The TPD is characterized by highly elevated *in situ* CDOM fluorescence in the central Arctic Ocean (higher CDOM than Laptev Sea surface waters), covering most of the Makarov Basin (Fig. 1). This circulation pattern is seen in the oceanographic cross sections (Fig. 3). The high salinity (>34.7), low CDOM, North Atlantic inflow to the Eurasian Basin consists of two main branches entering the Arctic Ocean through the eastern Fram Strait and the Barents Sea (e.g. Rudels, 2001). Waters coming from the Atlantic are characterized by low levels of CDOM absorbance and fluorescence and low terrigenous biomarker concentrations (TDLP9; Fig. 3). DOC concentrations were also lowest in these Atlantic influenced sections, particularly in the Nansen Basin (~50  $\mu\text{mol/L}$ ). Dissolved iron concentrations are slightly elevated near the bottom of the Franz Josef Victoria Trough seen in section A1 (~3 nmol/L, Fig. 3s), but were generally lower than in sections B and C which are influenced by river discharge. The locally elevated dFe concentrations near the bottom of section A1 likely originate from sediments since low TDLP9 concentrations exclude a riverine source (Fig. 3). These elevated dFe levels were concurrent with high concentrations of dissolved manganese which were attributed to benthic efflux in a previous study (Middag et al. 2011) and confirms sediment influence.

Section B, which stretches from the Kara Sea shelf break (82°N), crosses the Nansen and Amundsen Basins, the Lomonosov Ridge and Makarov Basin and ends over the Alpha Ridge in the Canada Basin (Fig. 1), is fundamentally different from section A. Section B can be characterized by slightly elevated *in situ* CDOM fluorescence in surface waters along the Kara Sea shelf break, low CDOM in the Nansen Basin, but very high CDOM concentrations within the TPD (Fig. 3).

The high CDOM fluorescence in the TPD is mirrored by elevated concentrations of several tDOM indicators, including TDLP9 concentrations (Fig. 3u), absorption coefficients  $a_{254}$  and  $a_{350}$  (Figs. 3g, k), lower  $S_{275-295}$  (Fig 3o), elevated PARAFAC component  $C_{482}$  (Fig.4), and DOC concentrations (Fig. 3w). The TPD feature is about 1000 km wide, spanning from the Gakkel Ridge to the Alpha Ridge based on *in situ* CDOM fluorescence. The dissolved iron concentrations in section B are also highly elevated in surface waters of the TPD (Fig. 3s) and closely resemble the distribution of CDOM and TDLP9 in the central Arctic Ocean.



The coastal section C begins on the Laptev Sea shelf (75°N) and follows the Gakkel Ridge into the Amundsen Basin (Fig. 1). CDOM is elevated in shelf station surface waters but not as much as in the TPD (Fig. 1). However, subsurface waters on the inner shelf have elevated levels of *in situ* CDOM fluorescence relative to surface waters (Stations 409-411), and they exceed concentrations seen in the TPD. The elevated CDOM fluorescence close to the bottom of the Laptev Sea shelf, at relatively high potential density comparing to the surface water, represents a unique CDOM feature in this data set (Fig. 3d). This feature was also reflected in high  $a_{254}$  and  $a_{350}$  values (Figs. 3h and 3l), low  $S_{275-295}$  values (Fig. 3p), elevated PARAFAC components  $C_{482}$ ,  $C_{428}$ ,  $C_{315}$ ,  $C_{302}$  (Fig. 4), and high TDLP9 concentrations (Fig. 3v). The concentration of dFe on the bottom of the Laptev Sea shelf exceeds 10 nmol/L, however, the peak does not extend to the shelf break (Fig. 3t). Shelf water concentrations of dFe were higher than in the TPD and generally coincided with *in situ* CDOM fluorescence and UV absorption at 254nm (Fig. 3).

The PARAFAC component  $C_{482}$  was found in several studies, and it is usually described as a terrigenous fluorophore in the Arctic Ocean (Walker et al. 2009; Chen et al. 2018; Gonçalves-Araujo et al. 2015, 2016). As such, the  $C_{482}$  component had the strongest correlation with *in situ* CDOM fluorescence and with TDLP9 concentrations. The maximum  $C_{482}$  fluorescence was observed in the TPD region, shown in section B (Fig. 4a), and in the Laptev Sea shelf bottom waters (Fig. 4b). Most of the PARAFAC components, except  $C_{408}$ , have a negative relationship with salinity. The distribution of  $C_{408}$  in the TPD region is different from all other components, showing a pronounced fluorescence signal in the upper halocline (isopycnals between 25.7 and 26.8 kg/m<sup>3</sup>; Fig. 4, top panel), at the depth of about 80 m on the Canadian side of section B (Fig. 4e). Relative to  $C_{482}$  and  $C_{428}$ , protein-like components  $C_{315}$  and  $C_{302}$  are more evenly distributed through the euphotic zone of section B (Fig. 4a, c), however, they also show elevated levels on the shallow Laptev shelf and within the surface of the TPD region (Fig. 4b, d).

The distribution of TDLP9 is generally similar to *in situ* CDOM fluorescence (Fig. 3) and DOC concentrations, with the highest values in the TPD region and in Laptev shelf bottom waters (inner shelf in section C). Elevated concentrations of TDLP9 were also observed in the halocline of the Makarov and Amundsen basins and in continental shelf waters. However, the

statistical relationship between lignin and in situ CDOM fluorescence was not as strong as for other proxies ( $R=0.77$ ,  $p < 0.00001$ ; Table 2) or as previously observed in the East Greenland Current ( $R=0.95$ ; Amon et al. 2003). Among all the tDOM proxies, the strongest correlation to TDLP9 was found with PARAFAC component  $C_{482}$ , demonstrating the usefulness of  $C_{482}$  for indicating a terrigenous signal in the Arctic Ocean ( $R=0.82$ ,  $p < 0.00001$ ; Table 2). Another, equally useful, optical proxy for tDOM was the absorption coefficient  $a_{254}$ , which is commonly used as a tracer of aromaticity and humic substances in freshwater systems (Weishaar et al. 2003).

Table 2. Pearson correlation matrix of TDLP9 concentrations and the parameters salinity, DOC, *in situ* CDOM fluorescence, absorption coefficients  $a_{254}$  and  $a_{350}$ , SUVA,  $S_{275-295}$ , and PARAFAC components

	Pearson correlation
Salinity	-0.75*
DOC	0.76*
CDOM	0.77*
$a_{254}$	0.82*
$a_{350}$	0.81*
SUVA	0.69*
$S_{275-295}$	-0.41
$C_{482}$	0.82*
$C_{428}$	0.77*
$C_{408}$	-0.07
$C_{315}$	0.5*
$C_{302}$	0.46*

\* $p < 0.01$

In terms of TDLP9 composition, the Nansen Basin has the highest p-hydroxyl to vanillyl phenol (P/V) ratios ( $>1.5$ ) due to the major influence of AW, which has the highest P/V ratio

269 (~1.9) among Arctic water masses (Kaiser et al. 2017). The P/V values are slightly elevated in  
 270 deeper water on the Laptev Sea shelf (>50 m, P/V = 1.35), which likely indicates the efflux of  
 271 degraded terrigenous DOM from sediments (Fig. 5). In contrast, the Makarov Basin surface layer  
 272 has the lowest P/V and syringyl to vanillyl phenol (S/V) ratios (<1), most likely due to the  
 273 influence of river discharge originating mostly from the Yenisei and Lena rivers, which have low  
 274 P/V and S/V ratios (Amon et al. 2012; Kaiser et al. 2017). The S/V ratios are also elevated in the  
 275 upper halocline (0.27-0.31) and the Laptev Sea shelf (<20 m), which could indicate the influence  
 276 of sea ice formation or a mix of tDOM from different Siberian rivers with varying S/V ratios  
 277 (Amon et al. 2012).

278 The strongest correlations to the distribution of dFe were found for  $a_{254}$  ( $R=0.87$ ,  $p < 0.00001$ )  
 279 and  $a_{350}$  ( $R=0.86$ ,  $p < 0.00001$ ; Table 3). Strong positive correlations of dFe were also found to  
 280 TDLP9 ( $R=0.74$ ,  $p < 0.00001$ ), all indicating that tDOM likely plays an important role in  
 281 delivering dissolved iron to the central Arctic Ocean. All CDOM fluorescence components but  
 282 one ( $C_{408}$ ), were positively correlated with dissolved iron (Table 3).

283 Table 3. Pearson correlation matrix between dFe and salinity, CDOM, absorption coefficients  
 284  $a_{254}$  and  $a_{350}$ , spectral slopes, SUVA, DOC, TDLP9, and PARAFAC components.

	Pearson correlation
Salinity	-0.72*
DOC	0.57*
TDLP9	0.74*
S/V	-0.49*
P/V	-0.61*
CDOM	0.76*
$a_{254}$	0.87*
$a_{350}$	0.86*
$S_{275-295}$	-0.27
SUVA	0.81*

C <sub>482</sub>	0.78*
C <sub>428</sub>	0.82*
C <sub>408</sub>	-0.23
C <sub>315</sub>	0.82*
C <sub>302</sub>	0.56*

\*p<0.01

## 4. Discussion

### 4.1 Origin of PARAFAC components

The five fluorescence components identified by the PARAFAC model (C<sub>482</sub>, C<sub>428</sub>, C<sub>408</sub>, C<sub>315</sub>, C<sub>302</sub>) have been described in previous studies (Table 4). The broad spectra of the visible wavelength (>400 nm) fluorescent components are often referred to as humic-like due to the dominance of this signal in hydrophobic organic matter extracts. The broad character is likely indicative of its complex chemical structure (Wünsch et al. 2015). The composition of visible wavelength fluorescence varies depending on DOM source (e.g. terrestrial vs aquatic) and exposure to degradation, with longer wavelength fluorescence being removed fastest (Murphy et al 2018). The narrow UV wavelength fluorescence of C<sub>315</sub> and C<sub>302</sub> is similar to that of simple aromatic compounds such as the amino acids tryptophan and tyrosine (free and combined in proteins), and benzoic acid derivatives (Wünsch et al. 2016). This is traditionally referred to as protein-like fluorescence and is present in the hydrophobic and hydrophilic fractions of DOM. These signals represent bioavailable DOM that is often absent in deep waters and far from DOM sources.

Using the OpenFluor database (Murphy et al. 2014), the spectral characteristics of each component can be matched with those from several previous Arctic studies (Table 4). The distributions of the components identified can be largely explained by the major hydrographic features of the Arctic Ocean.

Table 4. Spectral characteristics of the five components identified by PARAFAC and their comparison to previously identified components.

Ark-XXII/2	Description	Excitation max/	Similar components found in	References
------------	-------------	-----------------	-----------------------------	------------

2007		Emission max, nm	OpenFluor database	
C <sub>482</sub>	Humic-like, terrigenous	<240, 385/482	BERC3, Arctic Seawater C4, Arctic outflow C1, Lena2013 C2, Partners C2-4	Walker et al. 2009; Chen et al. 2018; Gonçalves-Araujo et al. 2015, 2018, Walker et al. 2013
C <sub>428</sub>	Humic-like	320(250)/ 428	BERC1, Lena2013 C1, Partners C1	Walker et al. 2009; Gonçalves-Araujo et al. 2015 Walker et al. 2013
C <sub>408</sub>	Humic-like	<240, 315/ 408	Arctic Seawater C2	Chen et al. 2018
C <sub>315</sub>	Tryptophan-like	295/315	Arctic Seawater C1, Partners C5	Chen et al. 2018; Walker et al. 2013
C <sub>302</sub>	Tyrosine-like, marine	<240, 275/ 302	BERC5, Arctic outflow C3	Walker et al. 2009 Gonçalves-Araujo et al. 2016

Of all PARAFAC components, C<sub>482</sub> was correlated strongest with lignin phenol concentrations (TDLP9) indicating a terrigenous source. Its spectral characteristics were equivalent to that found in river water and plumes of several major Arctic rivers (Table 4; Walker et al. 2009; Gonçalves-Araujo et al. 2015; Walker et al. 2013). C<sub>482</sub> was prevalent in the upper 60 m of the TPD, indicating a major contribution of river discharge to this current system crossing the Arctic Ocean, as suggested previously (Opsahl et al. 1999, Benner et al. 2005, Charette et al. 2020). Another visible wavelength peak, C<sub>428</sub>, had the highest fluorescence intensity of all components, accounting for half of the total fluorescence signal in the present as well as previous studies. It has a weaker correlation with lignin phenols than C<sub>482</sub> but was more strongly correlated with dissolved iron concentrations than the other fluorescent components. C<sub>428</sub> has also been identified in Arctic rivers (Table 4; Walker et al. 2009; Gonçalves-Araujo et al. 2015; Walker et al. 2013).

The C<sub>408</sub> component is most pronounced in the upper halocline extending into the Canada Basin, but it is also elevated near the Laptev Sea shelf break and below the terrigenous signal in the TPD (Fig. 4e, f). A similar fluorescence signal has been observed spreading from the Chukchi Sea shelf to the core of the upper halocline in the Canada Basin (Chen et al. 2018). This signal likely originates from organic matter decomposition in surface sediments on the shelf. The pronounced fluorescence signal far away from its apparent source on the Chukchi shelf indicates the intensity of the source (extensive productive shelf area) and its refractory nature.

The fluorescence intensity of this component was the lowest among all PARAFAC components which likely also reflects its large distance from the source region.

C<sub>315</sub> is similar to the tryptophan-like component described in Chen et al. (2018) and shows elevated concentrations on the shelf as well as in the TPD. The primary sources of this component are thought to be marine organic matter, including the decomposition of plankton-derived organic matter in shelf sediments. However, tannins and lignins, common constituents of terrestrial plants, are known for their protein-binding capability and could contribute to the fluorescence signature with an emission maximum near 315 nm (Maie et al. 2008). This would be consistent with the observed pattern of C<sub>315</sub> on the shelf and within the TPD. Previous studies demonstrated that fluorescence at these wavelengths can be highly correlated with lignin (Hernes et al. 2009; Osburn et al. 2016), but our data do not reflect such a relationship. A component with a similar fluorescence signature was found in Arctic rivers and appeared to be related to microbial activity (Walker et al. 2013). Similar to C<sub>315</sub>, component C<sub>302</sub> is thought to be linked to phytoplankton-derived organic matter and is correlated with amino-acid concentrations (Gonçalves-Araujo et al. 2016; Yamashita et al. 2020). This component is analogous to BERC5 (Walker et al. 2009) and Arctic outflow C3 (Gonçalves-Araujo et al. 2016).

#### 4.2 Distribution of biomarkers, optical properties and dissolved iron

The concentrations of dissolved iron are correlated with several indicators of organic matter sources based on optical properties and lignin phenols concentrations. The strongest relationships with dissolved iron concentrations were observed with absorption coefficients  $a_{254}$  and  $a_{350}$ , followed by the PARAFAC components C<sub>428</sub> and C<sub>315</sub>, SUVA, C<sub>482</sub>, and lignin phenols. The strong correlations of marine and terrigenous indicators (C<sub>315</sub>, C<sub>428</sub>, C<sub>482</sub>, TDLP9) with dissolved iron concentrations indicates that marine and terrigenous humic substances contribute to iron complexation. These observations are consistent with previous studies suggesting the association of dissolved iron with humic-like terrigenous organic ligands, particularly in the TPD, and humic-like marine ligands (Nakayama et al. 2011, Slagter et al. 2017, 2019; Sukekava et al. 2018; Laglera et al. 2019; Charette et al. 2020). The correlation between dissolved iron concentrations and C<sub>482</sub> was stronger than that with lignin phenols, possibly indicating the presence of other fluorescent terrigenous ligands, such as tannins, in the Eurasian Basin. The strong negative correlation between P/V of lignin phenols and dissolved iron concentrations

indicates recently discharged tDOM is an important source of iron-binding ligands in the study area. These observations are consistent with the strong correlation between lignin phenol concentrations and the natural radiocarbon content of DOC in the Arctic Ocean, indicating terrigenous DOC is mostly young in polar surface waters (Benner et al., 2004).

The observed correlations between dissolved iron concentrations and optical proxies of terrigenous and marine organic matter suggest a ubiquitous distribution of specific types of binding sites in dissolved organic molecules across the land-ocean aquatic continuum. Iron is a biologically vital trace metal that has very low solubility in oxygenated seawater. Iron solubility depends on complexation with organic molecules referred to as ligands, but little is known about the origins and molecular properties of ligands in natural waters. Ligands are categorized by their binding strength using a competitive ligand exchange–adsorptive cathodic stripping voltammetry technique (Rue and Bruland, 1995; Gledhill and Buck, 2012; Slagter et al. 2019). The number of iron-binding sites and their spatial arrangement are important features determining the binding strength of ligands, and it can range from monodentate to hexadentate complexation. Molecular size is another important characteristic influencing the binding strength of ligands, with higher-molecular-weight molecules typically having a greater number of binding sites, more flexible molecular geometries, and greater binding strength. Typically, one or two ligand types are reported,  $L_1$  ( $\log K'_{FeL} > 11$ ) is the stronger ligand class,  $L_2$  is weaker ligand class ( $\log K'_{FeL} < 11$ ), and  $L_{Total} = [L_1] + [L_2]$ . Some studies (summarized by Gledhill and Buck, 2012), suggested to use a definition for ligand classes based on the range of  $\log K'_{FeL}$  values reported in natural systems: “ $L_1$ ” for  $\log K'_{FeL} > 12$ , “ $L_2$ ” for  $\log K'_{FeL}$  varying between 11 and 12, and “ $L_3$ ”  $\log K'_{FeL} < 11$ . However, the different ligand classes are often hard to distinguish based on this definition (Gledhill and Buck, 2012; Gerringa et al. 2014; Hassler et al. 2017).

Siderophores are examples of strong binding ligands synthesized by bacteria to facilitate the acquisition of iron. Several siderophores have been chemically characterized and structurally defined (Mawji et al. 2008; Boiteau et al. 2013; Bundy et al. 2018; Sanchez et al. 2019). Hydroxamates are the most common class produced by heterotrophic bacteria and fungi, but despite the resistance to photodegradation (Barbeau et al. 2003), its concentrations in the ocean is too low (3-20 pM) to be a major ligand group (Mawji et al. 2008; Xu et al. 2020). Other organic molecules, however, can contain functional groups similar to the ones found in siderophores and

can serve as strong ligands by chance rather than by design. Examples of other functional groups are catechol type and carboxylate type, present in many naturally occurring biochemicals (Fig. 6). In addition, there are numerous other ligand types described in the literature (Crosa et al. 2004; Vraspir and Butler, 2009; Khan et al. 2018). For example, carbohydrates have carboxyl and hydroxyl groups that can have weak to strong affinities for iron, and carbohydrates are in much higher concentrations (nanomolar to micromolar) than carboxylate siderophores (Benner et al. 1992; Wang et al. 2006). Exopolysaccharides released from microorganisms can bind iron, thereby enhancing iron availability to eukaryotic phytoplankton that do not produce siderophores (Hassler et al. 2011; Hassler et al. 2017). Recent studies suggest that hydroxamate-like moieties are also present in particulate organic matter, but are a minor component of the particulate organic carbon (POC) pool (<1.5% of POC; Chuang et al. 2013). The POC pool of iron-binding molecules is dominated by aromatics, followed by black carbon-like and CRAM-like compounds, with minor contributions of aliphatics (Xu et al. 2020).

Humic substances are thought to include important iron-binding ligands in the ocean (Laglera and van den Berg 2009; Hassler et al. 2019), but little is known about the origins and molecular properties of these iron-binding humic ligands. Dissolved humic substances are an operationally-defined, diverse mixture of molecules that can be isolated from water using hydrophobic solid-phase extraction (Amador et al. 1990; Hedges et al. 1992). Nuclear magnetic resonance (NMR) spectroscopy of terrigenous humic substances isolated from the Amazon River system indicated high aromaticity and lignin-derived methoxyl carbon, as well as aliphatic and carboxyl carbon (Hedges et al. 1992). In contrast, NMR spectroscopic analyses of marine humic substances isolated from the Pacific Ocean indicated an abundance of carboxylated aliphatic molecules with a highly branched structure and low unsaturated carbon (Hedges et al. 1992). The elemental C:N ratio of the terrigenous humic substances was ~60 and that of the marine humic substances was ~36, indicating a relatively low nitrogen content in the molecules comprising humic substances (Hedges et al. 1992). Ultrahigh-resolution mass spectrometry (e.g. FT-ICR-MS) analyses of terrigenous and marine humic substances indicate a tremendous diversity of molecules, and in combination with NMR spectroscopy revealed an abundance of CRAM that could function as iron chelators (Hertkorn et al. 2006; Lam et al. 2007; Hertkorn et al. 2013; Lechtenfeld et al. 2014; Bundy et al. 2015). It was estimated that CRAM accounts for ~25% of the DOC in the ocean, making this an abundant and diverse class of molecules that are



distributed throughout the ocean water column (Fig. 6; Hertkorn et al. 2013). It appears humic substances and associated carboxyl-rich alicyclic molecules are very resistant to microbial degradation but can be susceptible to photodegradation (Shen and Benner, 2018), thereby potentially enhancing iron bioavailability in surface waters (Hassler et al. 2019).

The number of iron-binding sites in terrigenous humic-like ligands is variable (Krachler et al. 2015), but the aromaticity and iron-binding capacity of these humic substances seem positively related (Kikuchi et al. 2017). Arctic rivers are major sources of terrigenous humic substances that are rich in aromatic molecules, such as lignins and tannins, which likely play a role in iron complexation in river and coastal waters, including the TPD (Laglera and van den Berg, 2009; Laglera et al. 2019; Slagter et al. 2019). Like catechol type siderophores, lignin molecules are also enriched in catechol-type binding sites (Fig. 6). CRAM are thought to be degraded and altered forms of terpenoid compounds, such as sterols, hopanoids, and carotenoids, that are produced by terrestrial and marine organisms (Hertkorn et al. 2006; Lam et al. 2007), so they are potentially important ligands in freshwater and marine humic substances (Fig. 6). Carboxyl and hydroxyl functional groups are particularly abundant in CRAM of terrigenous and marine humic substances, and they are iron-binding sites (Hertkorn et al. 2006; Bundy et al. 2015). In addition, dissolved black carbon also contains carboxyl and hydroxyl functional groups and has been estimated to comprise ~10% of the DOC in fluvial discharge (Jaffé et al. 2013), but they have a relatively weak iron-binding capacity (Fig. 6).

The conditional stability constants of isolated terrigenous (Laglera and van den Berg, 2009) and marine humic substances (Hassler et al. 2019) are similar and can be explained by similar functional groups that bind to iron (Table 5 and Fig. 6). The covariation of iron and humic substances in the coastal waters and estuaries suggest the further transport of terrigenous humic substances and dFe into the open ocean (Laglera and van den Berg, 2009; Gerringa et al. 2015). This is consistent with the more recent finding that the mean iron-binding capacity of the open ocean samples indicate a similar range to terrestrial standards (Laglera et al. 2019; Whitby et al. 2020). It has been suggested that marine humic substances could account for 41% of the iron-binding ligands in deep waters and 7% in surface waters (Hassler et al. 2019). The conditional stability constants and concentrations of isolated terrigenous and marine humic substances are similar to those of L<sub>2</sub> type ligands reported in other studies (Table 5). This

confirms that CRAM and other types of potential ligands are ubiquitous in natural waters and the data in Table 5 and Fig. 6 provide strong evidence indicating diverse groups of molecules in humic substances can serve as iron-binding ligands and play a major role in maintaining bioavailable iron in the global ocean.

Measurements of ligand concentrations and conditional stability constants reported in natural waters indicate a ubiquitous distribution of specific types of binding sites in dissolved organic molecules across the land-ocean aquatic continuum (Table 5). Even in the Arctic Ocean, which is strongly influenced by tDOM, the differences in the conditional stability constants among different water masses were minimal (Thuróczy et al. 2011; Slagter et al. 2017). Slagter et al. (2017) reported that L<sub>1</sub> ligand type has a stronger affinity and higher concentration inside the TDP than in surface waters outside the TPD and in deep waters, which is likely due to the contribution of terrigenous ligands in humic substances. The L<sub>2</sub> ligand type also has a stronger affinity inside TPD, but it has higher concentrations in surface waters outside the TPD, implying that it has a marine origin.

The conditional stability constants and concentrations of ligands in the Barents Sea (Slagter et al., 2019), which is representative of the Atlantic water inflow to the Arctic, are similar to those of L<sub>2</sub> type ligands identified in the Arctic (Slagter et al., 2017; Table 5). Bering Sea water is representative of Pacific water inflow to the Arctic, and a strong correlation was observed between dissolved iron concentrations and L<sub>1</sub> concentrations in surface and subsurface waters over the Bering Sea shelf in proximity to terrigenous sources of iron (Buck and Bruland, 2007). These authors found that over 99% of the dissolved iron was complexed by L<sub>1</sub> ligands, and they did not find a significant correlation between dissolved iron and L<sub>2</sub> ligand concentrations. In the Bering Sea, dissolved iron was supplied to the surface waters of the Green Belt region from the shelf waters as FeL<sub>1</sub> complexes. Within this productive region, dissolved iron is depleted by phytoplankton while L<sub>1</sub> type ligand concentrations remained high (Buck and Bruland, 2007). Elevated concentrations of L<sub>1</sub> and L<sub>2</sub> ligands were also observed in the subsurface waters over the shelf, indicating sediments are an important source of these ligands. Among the marine and freshwater domains presented in Table 5, the conditional stability constants of iron-binding ligands are highest in the Arctic Ocean, especially in the TPD. This can not be explained by the presence of a single ligand type, but rather by the unique diversity of

ligand molecules with weaker binding strength, which in combination have the best chance of binding to dissolved iron, as similar functional groups might be present in different organic compounds.

#### 4.3 DOM and dissolved iron in relation to hydrographic features

It appears dissolved iron can bind to a large and diverse group of organic ligand molecules with terrigenous and marine origins. The distribution of DOM has been linked to water mass modification and circulation in the Arctic Ocean (Anderson and Amon 2015). Optical properties, biomarker, and dFe concentrations presented in this study reflect 3 major hydrographic (T/S) features of the Arctic Ocean. The most prominent distribution pattern is the Trans Polar Drift, with very high concentrations of dissolved iron, distinct optical properties, and high lignin phenol concentrations over 1500 km from riverine and shelf sources. The second most prominent distribution pattern is found associated with Eurasian shelf waters, which also had high concentrations of dissolved iron, optical properties, and lignin phenol concentrations derived from river and sediment sources. Sediments have been shown to be important sources of dissolved iron independent of river contributions on the Chuckchi shelf (Jensen et al. 2020). The third, less obvious hydrographic feature explaining the distribution of DOM and dissolved iron is the halocline layer, with slightly elevated concentrations of dissolved iron, distinct optical properties, and lower concentrations of lignin phenols.

The Arctic halocline separates the relatively warm Atlantic layer from the cold PML. The different halocline layers in the Arctic are complex and consist of many types of water masses coming from different sources and greatly vary in thickness (Rudels et al., 1996, 2001; Supplemental Table 1). The halocline structure in the Canada Basin differs from the Eurasian Basin stratification as the upper halocline (UHC) found in the Canadian Basin is almost absent from the Eurasian Basin (Anderson et al. 1994). In the Canada Basin, the UHC overlies the Eurasian Basin derived lower halocline (LHC). The halocline layers can be easily traced by elevated in situ CDOM fluorescence seen in section B (in high vertical resolution; Fig. 3). CDOM fluorescence originates on the Arctic shelves (river discharge and sediment release) and links the halocline-formation process to the shelves as originally suggested by Aagaard et al. (1981). We observed elevated levels of certain optical properties and dissolved iron in Eurasian halocline layers (supplemental Table 1), and a previous study related dFe concentrations to

elevated absorbance-based optical indicators of DOM in the UHC of the Canada Basin (Nakayama et al. 2011). While many DOM indicators used in this study were also found at elevated levels in the halocline, the only indicator unique to the halocline was PARAFAC component C<sub>408</sub>. This component has a pronounced peak in the upper halocline of the Canada Basin, near the Laptev Sea shelf break and directly underneath the TPD. The fluorescence signal of C<sub>408</sub> was lower than that of the other fluorophores. The C<sub>408</sub> component is most likely of marine origin and could be generated during organic matter decomposition in surface sediments on the shelf. The cruise only covered the northernmost portion of the Canada Basin, so it is difficult to clarify the role of C<sub>408</sub> as a dissolved iron ligand indicator, but C<sub>408</sub> fluorescence intensity increased along the Eurasian shelf-Canada Basin transect. The dissolved iron concentrations were much lower in the upper halocline compared to the TPD or the Laptev Sea shelf, indicating selective loss of dFe within the upper halocline, even though the optical properties indicate the ligands were probably present. The residence time of the halocline with respect to shelf inputs occurs on time scales of  $\leq 19\text{--}23$  years (Kipp et al. 2019), so we don't see the halocline as an important vector for dissolved iron transport to neighboring ocean basins.

The second major hydrographic feature of the Arctic Ocean influencing the distribution of dFe is the broad and shallow shelves, which receive very large freshwater discharge from rivers with high concentrations of DOM (Raymond et al. 2007, Amon et al. 2012) and dFe. In addition, the Eurasian shelves represent a location of net sea ice formation and shelf water modification (Bauch et al. 2016). The shallow, river dominated, shelves produce a diverse cocktail of organic molecules introduced by rivers and sediment-water exchanges that are reflected in the distribution of optical properties, the terrigenous biomarker, and associated dFe. The low salinity surface waters carry dFe-enriched tDOM along the Eurasian shelf from the Kara Sea to the Laptev Sea and the East Siberian Sea where it eventually gets entrained into the TPD. Within the TPD the dFe-enriched tDOM crosses the Arctic Ocean and is exported to the North Atlantic (Bauch et al. 2009, 2011). Much of the dFe-enriched Chuckchi and coastal Beaufort Sea shelf waters are swept towards the Canadian Archipelago by the Alaskan coastal current and flow into the Baffin Bay and the Labrador Sea (Fichot et al. 2013). The brine-enriched shelf waters produced during winter sea ice formation enter subsurface layers in the open Arctic and the dFe entrained in these layers will meet the fate described above for the halocline.

The Trans Polar Drift carries iron-enriched tDOM and sediment derived DOM from Eurasian rivers and shelves across the Arctic Ocean and becomes the East Greenland Current exporting the high CDOM-high tDOM to the North Atlantic (Amon et al. 2003, Benner et al. 2005). The TPD had high concentrations of dissolved iron and DOM near the North Pole, so it is likely that most of the dissolved iron and DOM is transported to the North Atlantic. Previous work has detected elevated concentrations of Arctic river CDOM and tDOM in surface waters of the Denmark Strait and the Irminger Sea (Amon et al. 2003, Benner et al. 2005) as well as in Denmark Strait Overflow Water, contributing to North Atlantic Deep Water (Benner et al. 2005). Elevated concentrations of dissolved iron were observed in the Western North Atlantic at depths between 800 and 2500 m, corresponding to Labrador Sea Water (Conway and John, 2014). Tonnard et al. (2020) also reported elevated iron concentrations within Denmark Strait Overflow Water, Iceland– Scotland-Ridge Overflow Water, and Upper Labrador Sea Water, and they attributed the elevated concentrations to iron-binding organic ligand complexes that were transported to the deep ocean by convection of water masses. This long-range transport of iron-rich Arctic shelf DOM may have a significant effect on primary production and the bioavailability of dissolved iron in North Atlantic surface waters and the Southern Ocean through the upwelling of North Atlantic Deep Water in the Southern Ocean (Gerringa et al. 2015; Klunder et al. 2011).

Table 5. Examples of published data on organic iron-binding ligands in the ocean, measured with the voltammetry techniques.

Region	Ligand predominant origin	Salinity	$\log K'_{FeL1}$	$\log K'_{FeL2}$	$\log K_{FeL3}'$	[L <sub>1</sub> ], nM	[L <sub>2</sub> ], nM	[L <sub>3</sub> ], nM	Reference
Suwannee River, GA, USA	Terrigenous (isolated humic acid)	0		11.1 ±0.2					Laglera and van den Berg (2009)
	Terrigenous (isolated fulvic acid)	0			10.6 ±0.2				
NW Atlantic Ocean (1000 m)	Marine (isolated humic substances)	35.5	12.26-12.4	11.64±0.45		1.,39-2.25	1.17		Hassler et al. (2020)

Mississippi River plume, LA, USA	Terrigenous	19.5-36.14	10.4-12.3			4.3-64.1			Powell and Wilson-Finelli (2003)
Transport from Peatland to Marine Waters (the Thurso river), Scotland	Terrigenous/Marine mix	0-34.7		11.05 $\pm 0.24$			96-21125		Muller and Cuscov (2017)
NE Atlantic surface coastal water	Terrigenous/Marine mix	28-35		10.23-11.97			46.5-573.2		Batchelli et al. (2010)
Arctic Ocean, Inside TPD ( $\leq 200$ m)	Terrigenous/Marine mix	34-34.2	13.3-13.6	11.6-11.76		1.58-2.29	1.26-2.76		Slagter et al. (2017)
Arctic Ocean, Outside TPD ( $\leq 200$ m)	Terrigenous/Marine mix	34.2-34.6	13.26 $\pm 0.71$	11.2 $\pm 0.17$		0.69 $\pm 0.27$	1.34 $\pm 0.56$		
Arctic Ocean/ >200m	Marine	34.6-35	13.14 $\pm 0.61$	11.16 $\pm 0.17$		0.62 $\pm 0.2$	1.28 $\pm 0.49$		
Barents Sea	Marine	28-33.5		11.2-12.1			1.26-2.14		Slagter et al. (2019)
Bering Sea (2-57 m)	Marine	31.6-31.9		11.1-12	9.7-10.8		0.43-18	1.2-15	Buck and Bruland (2007)
Arctic Ocean (0-4251m)	Marine	29.5-35	11.5-12.57				0.31-4.5		Thuróczy et al. (2011)

562

563

564 *Acknowledgments*

We thank Ursula Schauer, the chief scientist, the captain, scientists, and crew of the Polarstern for their support and help during the cruise and Gerhard Dieckmann for supplying lab space at the Alfred Wegener Institute. We thank Annie Whitley for her help with analyses in the lab. This work was funded by the National Science Foundation grant PLR-0425582 (R.M.W.A. and R.B.). The Netherlands GEOTRACES program in the International Polar Year (2007–2008) was supported by the Netherlands Organization for Scientific Research (Nederlandse Organisatie voor Wetenschappelijk Onderzoek, NOW; contract number 822.01.018 to L.J.A. Gerringa.). The manuscript benefited from suggestions by L.J.A. Gerringa and two anonymous reviewers.

## References

- Aagaard, K., Coachman, L. K., & Carmack, E., 1981. On the halocline of the Arctic Ocean. *Deep Sea Research Part A. Oceanographic Research Papers*, 28, 6, 529-545.
- Amador, J., Milne, P. J., Moore, C. A., & Zika, R. G., 1990. Extraction of chromophoric humic substances from seawater. *Marine Chemistry*, 29, 1-17.
- Amon, R. M. W., 2004. The role of dissolved organic matter for the Arctic Ocean carbon cycle, *In* “The Arctic Ocean Organic Carbon Cycle: Present and Past”, R. Stein, R.W. Macdonald, Eds., pp. 83-99. Springer.
- Amon, R. M. W., Rinehart, A. J., Duan, S., Louchouart, P., Prokushkin, A., Guggenberger, G., ... & McClelland, J. W., 2012. Dissolved organic matter sources in large Arctic rivers. *Geochimica et Cosmochimica Acta*, 94, 217-237.
- Amon, R. M. W., & Benner, R., 2003. Combined neutral sugars as indicators of the diagenetic state of dissolved organic matter in the Arctic Ocean. *Deep Sea Research Part I: Oceanographic Research Papers*, 50, 1, 151-169.
- Amon, R. M. W., Budeus, G., Meon, B., 2003. Dissolved organic carbon, DOC distribution and origin in the Nordic Seas: Exchanges with the Arctic Ocean and the North Atlantic. *J. Geophys. Res.-Oceans*: Vol. 108, No. C7,3221,doi:10.1029/2002JC001594.
- Anderson, L. G., & Amon, R. M. W., 2015. DOM in the Arctic Ocean. *In* Biogeochemistry of marine dissolved organic matter, pp. 609-633. *Academic Press*.
- Anderson, L. G., Andersson, P. S., Björk, G., Peter Jones, E., Jutterström, S., & Wåhlström, I., 2013. Source and formation of the upper halocline of the Arctic Ocean. *Journal of Geophysical Research: Oceans*, 118, 1, 410-421.
- Anderson, L. G., Björk, G., Holby, O., Jones, E. P., Kattner, G., Koltermann, K. P., ... & Swift, J., 1994. Water masses and circulation in the Eurasian Basin: Results from the Oden 91 expedition. *Journal of Geophysical Research: Oceans*, 99, C2, 3273-3283.
- Barbeau, K., Rue, E.L., Bruland, K.W. and Butler, A., 2001. Photochemical cycling of iron in the surface ocean mediated by microbial iron (III)-binding ligands. *Nature*, 413(6854), pp.409-413.
- Barbeau, K., Rue, E.L., Trick, C.G., Bruland, K.W. and Butler, A., 2003. Photochemical reactivity of siderophores produced by marine heterotrophic bacteria and cyanobacteria based on characteristic Fe (III) binding groups. *Limnology and Oceanography*, 48(3), pp.1069-1078.

Batchelli, S., F. L. Muller, K.-C. Chang, and C.-L. Lee, 2010, Evidence for strong but dynamic iron-humic colloidal associations in humic-rich coastal waters., *Environmental Science & technology*, 44, 22, 8485–90, doi:10.1021/es101081c.

Bauch, D., Cherniavskaia, E., & Timokhov, L., 2016. Shelf basin exchange along the Siberian continental margin: Modification of Atlantic Water and Lower Halocline Water. *Deep Sea Research Part I: Oceanographic Research Papers*, 115, 188-198.

Bauch, D., Hölemann, J., Andersen, N., Dobrotina, E., Nikulina, A., & Kassens, H., 2011. The Arctic shelf regions as a source of freshwater and brine-enriched waters as revealed from stable oxygen isotopes. *Polarforschung*, 80, 3, 127-140.

Benner, R., 2011. Loose ligands and available iron in the ocean. *Proceedings of the National Academy of Sciences*, 108, 3, 893-894.

Benner, R., 2011. Loose ligands and available iron in the ocean. *Proceedings of the National Academy of Sciences*, 108, 3, 893-894.

Benner, R., Benitez-Nelson, B., Kaiser, K., & Amon, R. M. W., 2004. Export of young terrigenous dissolved organic carbon from rivers to the Arctic Ocean. *Geophysical Research Letters*, 31, L05305, doi:10.1029/2003GL019251.

Benner, R., Louchouart, P., & Amon, R. M. W., 2005. Terrigenous dissolved organic matter in the Arctic Ocean and its transport to surface and deep waters of the North Atlantic. *Global Biogeochemical Cycles*, 19, 2.

Benner, R., Pakulski, J. D., McCarthy, M., Hedges, J. I., & Hatcher, P. G., 1992. Bulk chemical characteristics of dissolved organic matter in the ocean. *Science*, 255, 5051, 1561-1564.

Boiteau, R.M., Fitzsimmons, J.N., Repeta, D.J. and Boyle, E.A., 2013. Detection of iron ligands in seawater and marine cyanobacteria cultures by high-performance liquid chromatography-inductively coupled plasma-mass spectrometry. *Analytical chemistry*, 85(9), pp.4357-4362.

Buck, K. N., Lohan, M. C., Berger, C. J., & Bruland, K. W., 2007. Dissolved iron speciation in two distinct river plumes and an estuary: Implications for riverine iron supply. *Limnology and Oceanography*, 52, 2, 843-855.

Bundy, R. M., Boiteau, R. M., McLean, C., Turk-Kubo, K. A., McIlvin, M. R., Saito, M. A., ... & Repeta, D. J., 2018. Distinct siderophores contribute to iron cycling in the mesopelagic at station ALOHA. *Frontiers in Marine Science*, 5, 61.

Bundy, R.M., Abdulla, H.A., Hatcher, P.G., Biller, D.V., Buck, K.N. and Barbeau, K.A., 2015. Iron-binding ligands and humic substances in the San Francisco Bay estuary and estuarine-influenced shelf regions of coastal California. *Marine Chemistry*, 173, pp.183-194.

Charette, M. A., Kipp, L. E., Jensen, L. T., Dabrowski, J. S., Whitmore, L. M., Fitzsimmons, J. N., et al., 2020. The Transpolar Drift as a source of riverine and shelf-derived trace elements to the central Arctic Ocean. *Journal of Geophysical Research: Oceans*, 125, e2019JC015920. <https://doi.org/10.1029/2019JC015920>

Chen, M., Jung, J., Lee, Y. K., & Hur, J., 2018. Surface accumulation of low molecular weight dissolved organic matter in surface waters and horizontal off-shelf spreading of nutrients and humic-like fluorescence in the Chukchi Sea of the Arct

Chuang, C. Y., Santschi, P. H., Ho, Y. F., Conte, M. H., Guo, L., Schumann, D., ... & Li, Y. H., 2013. Role of biopolymers as major carrier phases of Th, Pa, Pb, Po, and Be radionuclides in settling particles from the Atlantic Ocean. *Marine Chemistry*, 157, 131-143. *Science of the Total Environment*, 639, 624-632.

Crosa, J. H., Mey, A. R., & Payne, S. M., Eds., 2004. Iron transport in bacteria, Vol. 410. Washington, DC: ASM press.



646 Fichot, C. G., & Benner, R., 2012. The spectral slope coefficient of chromophoric dissolved organic matter, S<sub>275–</sub>  
647 295 as a tracer of terrigenous dissolved organic carbon in river-influenced ocean margins. *Limnology and*  
648 *Oceanography*, 57, 5, 1453-1466.

649 Fichot, C. G., Kaiser, K., Hooker, S. B., Amon, R. M. W., Babin, M., Bélanger, S., ... & Benner, R., 2013. Pan-  
650 Arctic distributions of continental runoff in the Arctic Ocean. *Scientific reports*, 3, 1053.

651 Gerringa, L. J., Rijkenberg, M. J., Schoemann, V., Laan, P., & De Baar, H. J., 2015. Organic complexation of iron in  
652 the West Atlantic Ocean. *Marine Chemistry*, 177, 434-446.

653 Gerringa, L. J., Rijkenberg, M. J., Thuróczy, C. E., & Maas, L. R. (2014). A critical look at the calculation of the  
654 binding characteristics and concentration of iron complexing ligands in seawater with suggested improvements.  
655 *Environmental Chemistry*, 11(2), 114-136.

656 Gledhill, M., & Buck, K. N., 2012. The organic complexation of iron in the marine environment: a review. *Frontiers*  
657 *in microbiology*, 3, 69.

658 Gonçalves-Araujo, R., Granskog, M.A., Bracher, A., Azetsu-Scott, K., Dodd, P.A. and Stedmon, C.A., 2016. Using  
659 fluorescent dissolved organic matter to trace and distinguish the origin of Arctic surface waters. *Scientific*  
660 *reports*, 6, p.33978.

661 Gonçalves-Araujo, R., Stedmon, C., Kraberg, A., & Bracher, A., 2015. DYNAMICS OF DOM IN THE LENA  
662 DELTA REGION, SIBERIA REVEALED BY PARALLEL FACTOR ANALYSIS.

663 Hansell, D. A., 2005. Dissolved organic carbon reference material program. *Eos, Transactions American*  
664 *Geophysical Union*, 86, 35, 318-318.

665 Hassler, C. S., Schoemann, V., Nichols, C. M., Butler, E. C., & Boyd, P. W., 2011. Saccharides enhance iron  
666 bioavailability to Southern Ocean phytoplankton. *Proceedings of the National Academy of Sciences*, 108, 3,  
667 1076-1081.

668 Hassler, C. S., van den Berg, C. M., & Boyd, P. W., 2017. Toward a regional classification to provide a more  
669 inclusive examination of the ocean biogeochemistry of iron-binding ligands. *Frontiers in Marine Science*, 4, 19.

670 Hassler, C., Cabanes, D., Blanco-Ameijeiras, S., Sander, S. G., & Benner, R., 2020. Importance of refractory ligands  
671 and their photodegradation for iron oceanic inventories and cycling. *Marine and Freshwater Research*, 71, 3,  
672 311-320.

673 Hedges, J. I., Hatcher, P. G., Ertel, J. R., & Meyers-Schulte, K. J., 1992. A comparison of dissolved humic  
674 substances from seawater with Amazon River counterparts by <sup>13</sup>C-NMR spectrometry. *Geochimica et*  
675 *Cosmochimica Acta*, 56, 4, 1753-1757.

676 Helms, J. R., Stubbins, A., Ritchie, J. D., Minor, E. C., Kieber, D. J., & Mopper, K., 2008. Absorption spectral  
677 slopes and slope ratios as indicators of molecular weight, source, and photobleaching of chromophoric  
678 dissolved organic matter. *Limnology and Oceanography*, 53, 3, 955-969.

679 Hernes, P. J., Bergamaschi, B. A., Eckard, R. S., & Spencer, R. G., 2009. Fluorescence-based proxies for lignin in  
680 freshwater dissolved organic matter. *Journal of Geophysical Research: Biogeosciences*, 114, G4.

681 Hertkorn, N., Benner, R., Frommberger, M., Schmitt-Kopplin, P., Witt, M., Kaiser, K., ... & Hedges, J. I., 2006.  
682 Characterization of a major refractory component of marine dissolved organic matter. *Geochimica et*  
683 *Cosmochimica Acta*, 70, 12, 2990-3010.

684 Hertkorn, N., Harir, M., Koch, B., Michalke, B., & Schmitt-Kopplin, P., 2013. High-field NMR spectroscopy and  
685 FTICR mass spectrometry: powerful discovery tools for the molecular level characterization of marine  
686 dissolved organic matter. *Biogeosciences*, 10, 1583-1624. Jaffé, R., Ding, Y., Niggemann, J., Vähätalo, A. V.,

687 Stubbins, A., Spencer, R. G., ... & Dittmar, T., 2013. Global charcoal mobilization from soils via dissolution  
688 and riverine transport to the oceans. *Science*, 340, 6130, 345-347.

689 Jensen, L.T., Morton, P., Twining, B.S., Heller, M.I., Hatta, M., Measures, C.I., John, S., Zhang, R., Pinedo-  
690 Gonzalez, P., Sherrell, R.M., Fitzsimmons, J.N. A comparison of marine Fe and Mn cycling: U.S.  
691 GEOTRACES GN01 Western Arctic case study. In review at *Geochimica et Cosmochimica Acta*.

692 Kaiser, K., Benner, R., Amon, R. M. W., 2017, The fate of terrigenous dissolved organic carbon on the Eurasian  
693 shelves and export to the North Atlantic, *J. Geophys. Res. Oceans*, 122, 4–22, doi:10.1002/2016JC012380.

694 Kaiser, K., Canedo-Oropeza, M., McMahon, R., & Amon, R. M. W., 2017. Origins and transformations of dissolved  
695 organic matter in large Arctic rivers. *Scientific reports*, 7, 1, 13064.

696 Khan, A., Singh, P., & Srivastava, A., 2018. Synthesis, nature and utility of universal iron chelator–Siderophore: A  
697 review. *Microbiological research*, 212, 103-111.

698 Kikuchi, T., Hatakeyama, K., & Morison, J. H., 2004. Distribution of convective lower halocline water in the  
699 eastern Arctic Ocean. *Journal of Geophysical Research: Oceans*, 109, C12. Morison, J., Kwok, R., Peralta-  
700 Ferriz, C., Alkire, M., Rigor, I., Andersen, R., & Steele, M., 2012. Changing arctic ocean freshwater pathways.  
701 *Nature*, 481, 7379, 66.

702 Klunder, M. B., Laan, P., Middag, R., De Baar, H. J. W., & Van Ooijen, J. C., 2011. Dissolved iron in the Southern  
703 Ocean , Atlantic sector. *Deep Sea Research Part II: Topical Studies in Oceanography*, 58, 25-26, 2678-2694.

704 Klunder, M.B., Bauch, D., Laan, P., De Baar, H.J.W., van Heuven, S., Ober, S., 2012a Dissolved iron in the Arctic  
705 shelf seas and surface waters of the central Arctic Ocean: Impact of Arctic river water and ice-melt. *Journal of*  
706 *Geophysical Research: Oceans* 117, C01027,  
707 [https://urldefense.com/v3/\\_\\_https://doi.org/10.1029/2011JC007133\\_\\_;!!KwNVnqRv!TXJ3dnn7\\_nX\\_4ixhjFIG](https://urldefense.com/v3/__https://doi.org/10.1029/2011JC007133__;!!KwNVnqRv!TXJ3dnn7_nX_4ixhjFIGQ378Bgni_YsxqC14u2bOiXCdJhVcrC11uzFNe3zqgw$)  
708 [Q378Bgni\\_YsxqC14u2bOiXCdJhVcrC11uzFNe3zqgw\\$](https://urldefense.com/v3/__https://doi.org/10.1029/2011JC007133__;!!KwNVnqRv!TXJ3dnn7_nX_4ixhjFIGQ378Bgni_YsxqC14u2bOiXCdJhVcrC11uzFNe3zqgw$)

709 Klunder, Maarten B; Bauch, Dorothea; Laan, Patrick; de Baar, Hein J W; van Heuven, Steven; Ober, Sven , 2012b:  
710 Dissolved iron measurements from 44 stations in the shallow Arctic Ocean waters and Shelf Sea's during  
711 POLARSTERN cruise ARK-XXII/2. PANGAEA,  
712 [https://urldefense.com/v3/\\_\\_https://doi.org/10.1594/PANGAEA.780543\\_\\_;!!KwNVnqRv!TXJ3dnn7\\_nX\\_4ixhj](https://urldefense.com/v3/__https://doi.org/10.1594/PANGAEA.780543__;!!KwNVnqRv!TXJ3dnn7_nX_4ixhjFIGQ378Bgni_YsxqC14u2bOiXCdJhVcrC11uzFKEh4RyQ$)  
713 [FIGQ378Bgni\\_YsxqC14u2bOiXCdJhVcrC11uzFKEh4RyQ\\$](https://urldefense.com/v3/__https://doi.org/10.1594/PANGAEA.780543__;!!KwNVnqRv!TXJ3dnn7_nX_4ixhjFIGQ378Bgni_YsxqC14u2bOiXCdJhVcrC11uzFKEh4RyQ$) . Supplement to: Klunder, MB et al., 2012a

714 Krachler, R., F. von der Kammer, F. Jirsa, A. Süphandag, R. F. Krachler, C. Plessl, M. Vogt, B. K. Keppler, and T.  
715 Hofmann, 2012, Nanoscale lignin particles as sources of dissolved iron to the ocean, *Global Biogeochem.*  
716 *Cycles*, 26, doi:10.1029/2012GB004294.

717 Krachler, R., Krachler, R. F., Wallner, G., Hann, S., Laux, M., Recalde, M. F. C., ... & Keppler, B. K., 2015. River-  
718 derived humic substances as iron chelators in seawater. *Marine chemistry*, 174, 85-93.

719 Laglera, L. M., & van den Berg, C. M., 2009. Evidence for geochemical control of iron by humic substances in  
720 seawater. *Limnology and Oceanography*, 54, 2, 610-619.

721 Laglera, L. M., Sukekava, C., Slagter, H. A., Downes, J., Aparicio-Gonzalez, A., & Gerringa, L. J., 2019. First  
722 quantification of the controlling role of humic substances in the transport of iron across the surface of the Arctic  
723 Ocean. *Environmental science & technology*, 53, 22, 13136-13145.

724 Lam, B., Baer, A., Alae, M., Lefebvre, B., Moser, A., Williams, A., & Simpson, A. J., 2007. Major structural  
725 components in freshwater dissolved organic matter. *Environmental Science & Technology*, 41, 24, 8240-8247.

726 Lechtenfeld, O. J., Kattner, G., Flerus, R., McCallister, S. L., Schmitt-Kopplin, P., & Koch, B. P., 2014. Molecular  
727 transformation and degradation of refractory dissolved organic matter in the Atlantic and Southern Ocean.  
728 *Geochimica et Cosmochimica Acta*, 126, 321-337.

729 Louchouart, P., Opsahl, S., & Benner, R., 2000. Isolation and quantification of dissolved lignin from natural waters  
730 using solid-phase extraction and GC/MS. *Analytical chemistry*, 72, 13, 2780-2787.

731 Maie, N., Pisani, O., & Jaffé, R., 2008. Mangrove tannins in aquatic ecosystems: their fate and possible influence on  
732 dissolved organic carbon and nitrogen cycling. *Limnology and Oceanography*, 53, 1, 160-171.

733 Mawji, E., Gledhill, M., Milton, J. A., Tarran, G. A., Ussher, S., Thompson, A., ... & Achterberg, E. P., 2008.  
734 Hydroxamate siderophores: occurrence and importance in the Atlantic Ocean. *Environmental science &*  
735 *technology*, 42, 23, 8675-8680.

736 Middag, R., P. Laan, H. J. W. de Baar, M. B. Klunder, 2011, Fluvial and hydrothermal input of manganese into the  
737 Arctic Ocean, *Geochim. Cosmochim. Acta*, 75, 2393–2408, doi:10.1016/j.gca.2011.02.011

738 Murphy K.R., Stedmon C.A., Graeber D. and R. Bro, Fluorescence spectroscopy and multi-way techniques.  
739 PARAFAC, , 2013, *Anal. Methods*, DOI:10.1039/c3ay41160e

740 Murphy, K. R., Timko, S. A., Gonsior, M., Powers, L. C., Wünsch, U. J., & Stedmon, C. A., 2018. Photochemistry  
741 illuminates ubiquitous organic matter fluorescence spectra. *Environmental science & technology*, 52, 19, 11243-  
742 11250.

743 Murphy, K.R., Stedmon, C.A., Wenig, P. and Bro, R., 2014. OpenFluor—an online spectral library of auto-  
744 fluorescence by organic compounds in the environment. *Analytical Methods*, 6, 3, pp.658-661.

745 Nakayama, Y., Fujita, S., Kuma, K., & Shimada, K., 2011. Iron and humic-type fluorescent dissolved organic matter  
746 in the Chukchi Sea and Canada Basin of the western Arctic Ocean. *Journal of Geophysical Research: Oceans*,  
747 116, C7.

748 Opsahl, S., & Benner, R., 1997. Distribution and cycling of terrigenous dissolved organic matter in the ocean.  
749 *Nature*, 386, 6624, 480.

750 Opsahl, S., Benner, R., Amon, R. M. W., 1999: Major flux of terrigenous dissolved organic matter through the  
751 Arctic Ocean. *Limnology & Oceanography*: 44: 2017-2023

752 Osburn, C. L., Boyd, T. J., Montgomery, M. T., Bianchi, T. S., Coffin, R. B., & Paerl, H. W., 2016. Optical proxies  
753 for terrestrial dissolved organic matter in estuaries and coastal waters. *Frontiers in Marine Science*, 2, 127.

754 Rijkenberg M. J. A., Slagter H. A., Rutgers van der Loeff M., van Ooijen J & Gerringa L. J. A. , 2018 Dissolved Fe  
755 in the Deep and Upper Arctic Ocean with a Focus on Fe Limitation in the Nansen Basin. *Front. Mar. Sci.* 5:88.  
756 doi: 10.3389/fmars.2018.00088

757 Rudels, B., 2001. Ocean Current: Arctic Basin Circulation. In J. Steele, S. Thorpe, & K. Turekian, Eds.,  
758 *Encyclopedia of Ocean Sciences* , pp. 177-187

759 Rudels, B., Anderson, L. G., Jones, E. P., 1996. Formation and evolution of the surface mixed layer and halocline of  
760 the Arctic Ocean. *J. Geophys. Res.* **101**, 8807-8821.

761 Rue, E. L., & Bruland, K. W., 1995. Complexation of iron, III by natural organic ligands in the Central North  
762 Pacific as determined by a new competitive ligand equilibration/adsorptive cathodic stripping voltammetric  
763 method. *Marine chemistry*, 50, 1-4, 117-138.

764 Sanchez, N., Peterson, C. K., Gonzalez, S. V., Vadstein, O., Olsen, Y., & Ardelan, M. V., 2019. Effect of  
765 hydroxamate and catecholate siderophores on iron availability in the diatom *Skeletonema costatum*:  
766 Implications of siderophore degradation by associated bacteria. *Marine Chemistry*, 209, 107-119.

767 Schauer, U., 2008. The expedition ARKTIS-XXII/2 of the Research Vessel ‘Polarstern’ in 2007. Berichte zur  
768 Polar- und Meeresforschung – Reports on Polar and Marine Research, vol. 579, 271pp

769 Schlitzer, R., Anderson, R., Masferrer Dodas, E., Lohan, M.C., Geibert, W., et al..The GEOTRACES Intermediate  
770 Data Product 2017. Chemical Geology, Elsevier, 2018, Volume 493,pp.210-223.  
771 10.1016/j.chemgeo.2018.05.040. hal-01819333

772 Shen, Y., & Benner, R., 2018. Mixing it up in the ocean carbon cycle and the removal of refractory dissolved  
773 organic carbon. *Scientific reports*, 8, 1, 1-9.

774 Slagter, H. A., Laglera, L. M., Sukekava, C., & Gerringa, L. J., 2019. Fe-binding organic ligands in the humic-rich  
775 TransPolar Drift in the surface Arctic Ocean using multiple voltammetric methods. *Journal of Geophysical*  
776 *Research: Oceans*, 124, 3, 1491-1508.

777 Slagter, H. A., Reader, H. E., Rijkenberg, M. J. A., Van Der Loeff, M. R., de Baar, H. J. W., & Gerringa, L. J. A.,  
778 2017. Organic Fe speciation in the Eurasian Basins of the Arctic Ocean and its relation to terrestrial DOM.  
779 *Marine Chemistry*, 197, 11-25.

780 Stedmon, C. A., Amon, R. M. W., Rinehart, A. J., & Walker, S. A., 2011. The supply and characteristics of colored  
781 dissolved organic matter, CDOM in the Arctic Ocean: Pan Arctic trends and differences. *Marine Chemistry*,  
782 124, 1-4, 108-118.

783 Stedmon, C. A., Markager, S., & Kaas, H., 2000. Optical properties and signatures of chromophoric dissolved  
784 organic matter, CDOM in Danish coastal waters. *Estuarine, Coastal and Shelf Science*, 51, 2, 267-278.

785 Sukekava, C., Downes, J., Slagter, H. A., Gerringa, L. J., & Laglera, L. M., 2018. Determination of the contribution  
786 of humic substances to iron complexation in seawater by catalytic cathodic stripping voltammetry. *Talanta*,  
787 189, 359-364.

788 Thuróczy, C. E., Gerringa, L. J. A., Klunder, M., Laan, P., Le Guitton, M., & De Baar, H. J. W., 2011. Distinct  
789 trends in the speciation of iron between the shallow shelf seas and the deep basins of the Arctic Ocean. *Journal*  
790 *of Geophysical Research: Oceans*, 116, C10.

791 Tonnard, M., Planquette, H., Bowie, A., Van Der Merwe, P., Gallinari, M., de Gésincourt, F. D., ... & Tréguer, P.,  
792 2020. Dissolved iron in the North Atlantic Ocean and Labrador Sea along the GEOVIDE section,  
793 GEOTRACES section GA01. *Biogeosciences*, 17, 4, 917-943.

794 Vraspir JM, Butler A, 2009 Chemistry of marine ligands and siderophores. *Annu Rev MarSci*1:43–63.

795 Walker, S. A., Amon, R. M. W., & Stedmon, C. A., 2013. Variations in high-latitude riverine fluorescent dissolved  
796 organic matter: A comparison of large Arctic rivers. *Journal of Geophysical Research: Biogeosciences*, 118, 4,  
797 1689-1702.

798 Walker, S.A., Amon, R. M. W., Stedmon, C., Duan, S.W. Louchouart, P., 2009. The use of PARAFAC modeling to  
799 trace terrestrial dissolved organic matter and fingerprint water masses in coastal Canadian Arctic surface waters.  
800 *J. Geophys. Res.* **114**, doi:10.1029/2009jg000990.

801 Wang, D., Henrichs, S. M., & Guo, L., 2006. Distributions of nutrients, dissolved organic carbon and carbohydrates  
802 in the western Arctic Ocean. *Continental Shelf Research*, 26, 14, 1654-1667.

803 Weishaar, J. L., Aiken, G. R., Bergamaschi, B. A., Fram, M. S., Fujii, R., & Mopper, K., 2003. Evaluation of  
804 specific ultraviolet absorbance as an indicator of the chemical composition and reactivity of dissolved organic  
805 carbon. *Environmental science & technology*, 37, 20, 4702-4708.

806 Whitby, H., Planquette, H., Cassar, N., Bucciarelli, E., Osburn, C. L., Janssen, D. J., ... & Sarthou, G., 2020. A call  
807 for refining the role of humic-like substances in the oceanic iron cycle. *Scientific Reports*, 10.

808 Wünsch U. J., Murphy, K. R. and Stedmon, C. A., 2015. Fluorescence Quantum Yields of Natural Organic Matter  
809 and Organic Compounds: Implications for the Fluorescence-based Interpretation of Organic Matter  
810 Composition. *Front. Mar. Sci.* 2: 98. doi: 10.3389/fmars.2015.00098

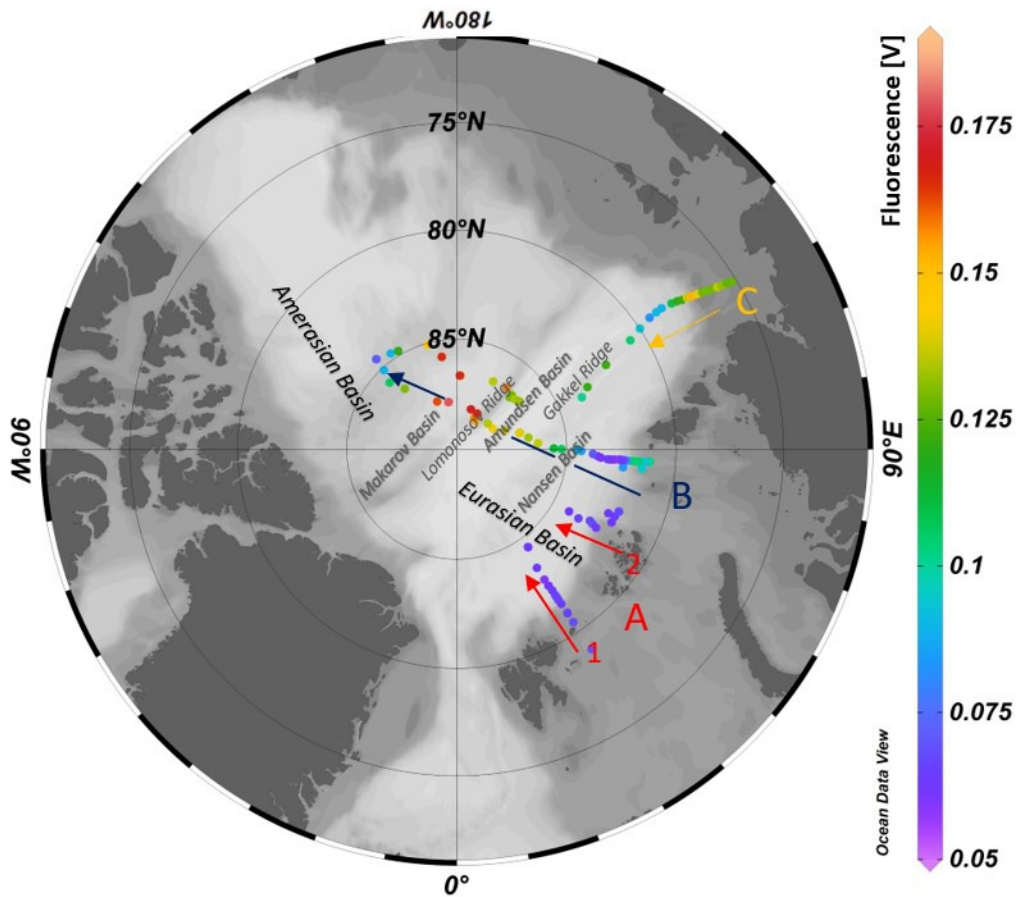
811 Wünsch, U. J., Murphy, K. R., & Stedmon, C. A., 2016. Corrigendum: Fluorescence Quantum Yields of Natural  
812 Organic Matter and Organic Compounds: Implications for the Fluorescence-based Interpretation of Organic  
813 Matter Composition. *Frontiers in Marine Science*, 3, 9.

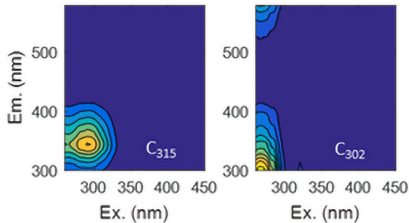
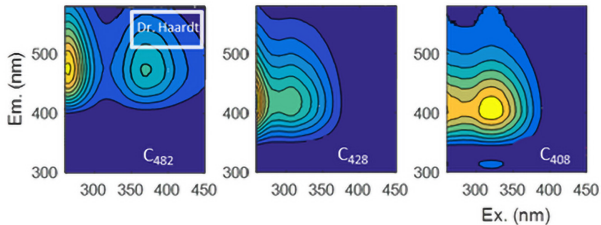
814 Xu, C., Lin, P., Sun, L., Chen, H., Xing, W., Kamalanathan, M., ... & Santschi, P. H., 2020. Molecular nature of  
815 marine particulate organic iron-carrying moieties revealed by electrospray ionization Fourier-transform ion  
816 cyclotron resonance mass spectrometry, ESI-FTICRMS. *Frontiers in Earth Science*, 8, 266.

817 Yamashita, Y., Nishioka, J., Obata, H., & Ogawa, H., 2020. Shelf humic substances as carriers for basin-scale iron  
818 transport in the North Pacific. *Scientific reports*, 10, 1, 1-10.

819 Yan, G., & Kaiser, K., 2018. A rapid and sensitive method for the analysis of lignin phenols in environmental  
820 samples using ultra-high performance liquid chromatography-electrospray ionization-tandem mass spectrometry  
821 with multiple reaction monitoring. *Analytica chimica acta*, 1023, 74-80.

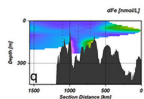
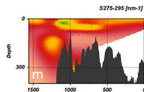
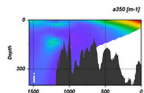
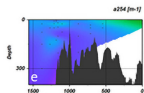
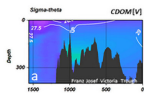
822 Yan, G., K. Kaiser., 2018. Ultra-low Sample Volume Cupric Sulfate Oxidation Method for the Analysis of  
823 Dissolved Lignin. *Anal. Chem.*, DOI: 10.1021/acs.analchem.8b01867, 68, 1-2, 59-70





## Section A1

(Atlantic water inflow region)

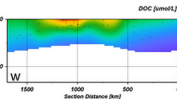
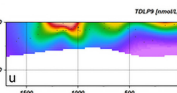
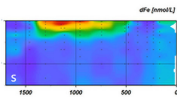
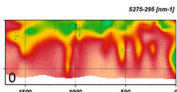
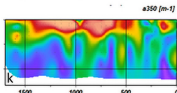
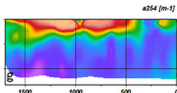
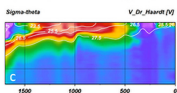


## Section A2



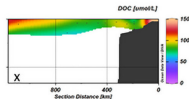
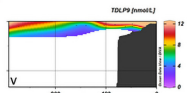
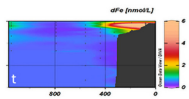
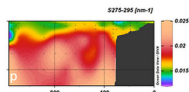
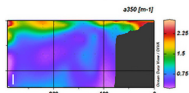
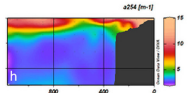
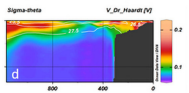
## Section B

(Transpolar Drift region)



## Section C

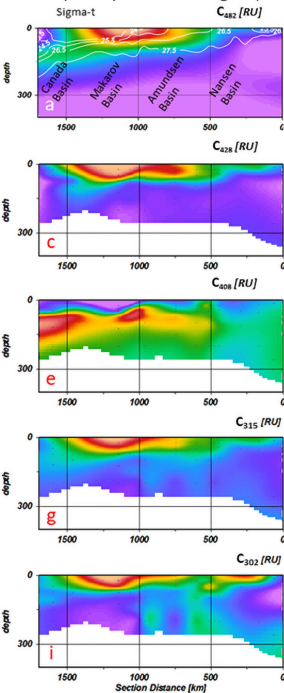
(Laptev Sea Shelf)





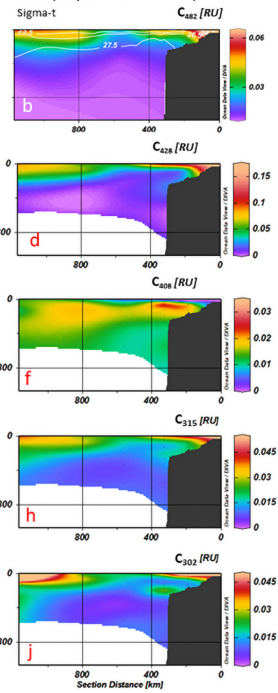
## Section B

(Transpolar Drift region)

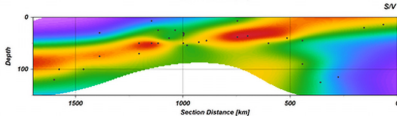
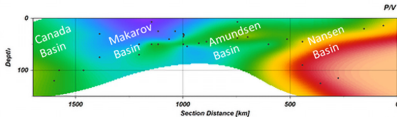


## Section C

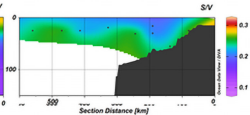
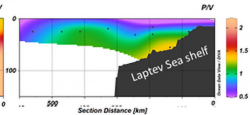
(Laptev Sea Shelf)



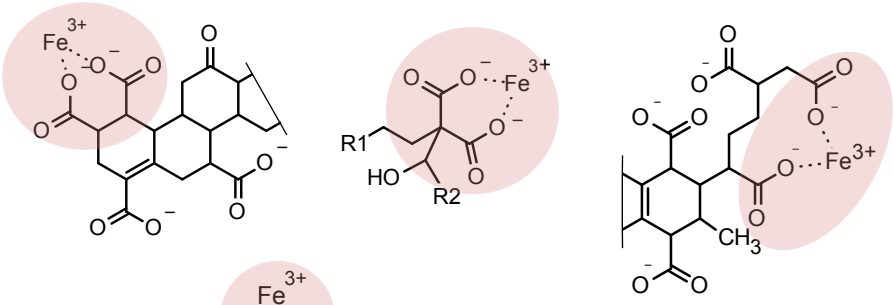
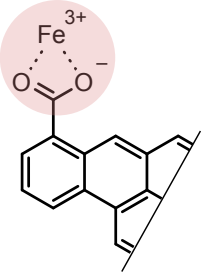
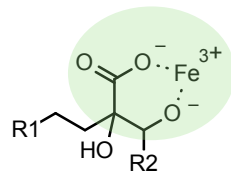
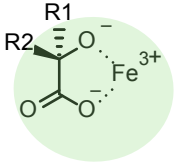
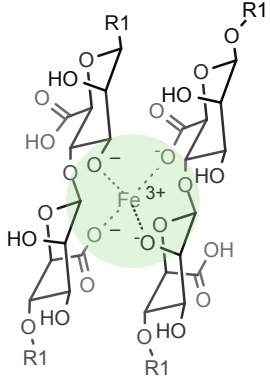
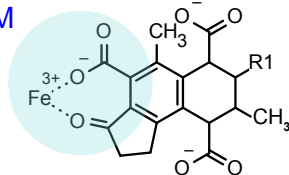
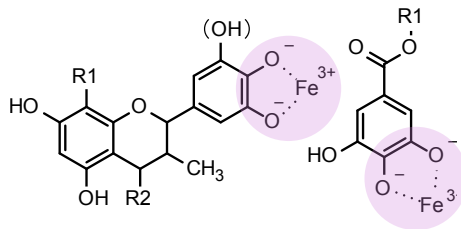
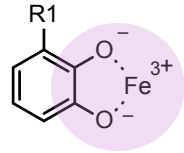
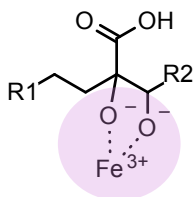
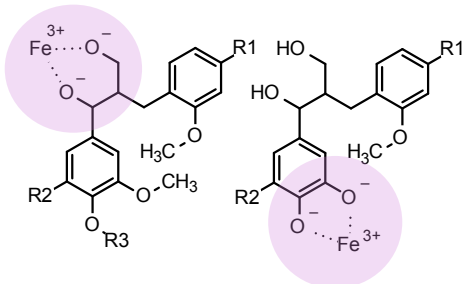
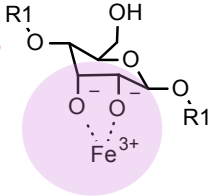
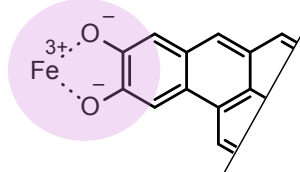
## Section B



## Section C



Functional groups for Fe(III) binding	Representative compound classes with structural examples	Origin	Bonding type and affinity
---------------------------------------	--	--------	---------------------------

<p>Carboxyl</p> $R1-C(=O)OH$	<p>CRAM</p> 	<p>marine and terrestrial</p>	<p>Bi- or multidentate</p> <p>weak to strong</p>
	<p>Dissolved black carbon</p> 	<p>marine and terrestrial</p>	<p>Bi- or multidentate</p> <p>weak</p>
<p>Hydroxyl/ carboxyl</p> $R1-OH \quad HO-C(=O)R2$	<p>CRAM</p>  <p>Siderophores (carboxylate type)</p>  <p>Carbohydrates</p> 	<p>marine and terrestrial</p>	<p>Multidentate</p> <p>weak to strong</p>
<p>Carbonyl/ carboxyl</p> $R1-C(=O)R2 \quad HO-C(=O)R2$	<p>CRAM</p> 	<p>marine and terrestrial</p>	<p>Bi- or multidentate</p> <p>weak to strong</p>
<p>Hydroxyl</p> $R1-OH$	<p>Tannins (condensed/ hydrolyzable types)</p>  <p>Siderophores (catechol type)</p>  <p>CRAM</p>  <p>Lignins</p>  <p>Carbohydrates</p>  <p>Dissolved black carbon</p> 	<p>terrestrial</p>	<p>Bi- or multidentate</p> <p>weak to strong</p>
		<p>marine</p>	<p>Bi- or multidentate</p> <p>weak to strong</p>
		<p>marine and terrestrial</p>	<p>Bi- or multidentate</p> <p>weak to strong</p>